Nanoscale Advances

ROYAL SOCIETY OF CHEMISTRY

PAPER

View Article Online
View Journal | View Issue

Cite this: *Nanoscale Adv.*, 2024, **6**, 1001

Nanodiamond-structured zinc composite coatings with strong bonding and high load-bearing capacity†

Shikha Awasthi, *[a] Blanca Prior Palomero,[b] Ankur Srivastava,*[c] S. Selvaraj[d] and Sarvesh Kumar Pandey*[ae]

The aerospace and automotive industries find that relying solely on the intrinsic resistance of alloys is inadequate to safeguard aircraft and automotive structural components from harsh environmental conditions. While it is difficult to attribute accidents exclusively to coating failure due to the involvement of multiple factors, there are instances where defects in the coating initiate a wear or degradation process, leading to premature and unplanned structural failures. Metallic coatings have been introduced to protect the aircraft mainly from wear due to the extreme temperatures and moisture exposure during their service life. Bare metallic coatings have a limited lifespan and need to be replaced frequently. Herein, the strength and wear resistance of zinc (Zn) coating is enhanced using varying concentrations of diamond particles as an additive in the Zn matrix (Zn-D). The dispersion strengthening mechanism is attributed to the high hardness (70 HRC), and reduced friction-of-coefficient (0.21) and dissipation energy (4.6×10^{-4} J) of electrodeposited Zn-D7.5 (7.5 g l^{-1} of diamond concentration) composite coating. Moreover, enhanced wear resistance with minimum wear volume (1.12×10^{-3} mm^3) and wear rate (1.25×10^{-3} mm^3 N^{-1} m^{-1}) of the Zn-D7.5 composite coating resulted in perfect blending of diamond with Zn. The improved hardness and wear resistance for Zn-D7.5 (optimum 7.5 g l^{-1} diamond concentration) is due to the steadiness between well-dispersed diamonds in Zn and enrichment in load-bearing ability due to the incorporation of diamond particles. Electronic structure calculations on the zinc-diamond composite models (two configurations adopted) have been performed using the density functional theory (DFT) approach, and the *in silico* studies appeared to facilitate meaningful and evocative outcomes. Zn-doped diamond (C_{10}@Zn) without hydrogen (H) atoms (binding energy: 418 kcal mol^{-1}, *i.e.* showing an endothermic reaction and thermodynamically not favourable) was detected to be more stable than the Zn-doped diamond ($C_{10}H_{16}$@Zn) consisting of hydrogen (H) atoms (binding energy: −33.3 kcal mol^{-1}, *i.e.* showing an exothermic reaction and thermodynamically preferable). Thus, a composite coating of zinc and diamond can be a suitable candidate for the aerospace and automotive industries.

Received 22nd September 2023
Accepted 21st December 2023

DOI: 10.1039/d3na00809f

rsc.li/nanoscale-advances

1. Introduction

Wear is a detrimental cause that leads to irreversible mutilation of the external surface of aircraft and automobiles.[1] Erosion wear has been recognized as the prime reason for several accidents, which have instigated the death of thousands of people.[2–4] As the aerospace industry introduces materials with enhanced strength and damage tolerance, there is an increased focus on their susceptibility to wear, especially since these materials often exhibit reduced resistance to fatigue wear attacks.[5,6] A key goal in achieving a long service life in such a demanding environment should include improved durability and life prediction of the coating.[7] A well-selected coating can yield significant benefits in terms of cost savings for maintenance and reparation while also providing enhanced protection against wear and corrosion.[8]

Until the present time, cadmium plating was widely used in the aerospace industry because of its wear resistance and excellent self-lubricating properties. Despite the advantages, there is a global trend towards replacing these coatings due to heightened environmental concerns and stringent regulations,

[a]*Department of Chemistry, Manipal University Jaipur, 303007, India. E-mail: shikha.awasthi@jaipur.manipal.edu*

[b]*Universidad Politécnica de Madrid, Madrid, Spain*

[c]*Department of Mechanical Engineering, Manipal University Jaipur, India, 303007. E-mail: ankur.srivastava@jaipur.manipal.edu*

[d]*Department of Physics, Saveetha School of Engineering, Saveetha Institute of Medical and Technical Sciences, Thandalam, Chennai 602105, Tamil Nadu, India*

[e]*Department of Chemistry, Maulana Azad National Institute of Technology, Bhopal, 462003, India. E-mail: spsarvesh22@gmail.com*

† Electronic supplementary information (ESI) available. See DOI: https://doi.org/10.1039/d3na00809f

as cadmium is a heavy toxic metal that causes significant environmental and health issues. Additionally, certain problems such as potential hydrogen embrittlement in high-strength alloys, incompatibility with titanium and hydraulic oils, and corrosion problems in acidic and ammonium salt-containing environments have prompted the exploration of alternative coating solutions.[9,10] A variety of commercial coatings are currently available as a suitable alternative to cadmium plating. Outstanding mechanical properties combined with wear resistance have prompted the investigation of metallic-ceramic coatings.[11,12] These coatings are created by depositing a mixture of metal and ceramic particles onto the surface of a substrate using various deposition techniques. Coating involves the application of an additional material to cover the surface of a component to improve its surface properties. Zinc is employed to increase the service life of components and improve their mechanical and tribological properties. The weldability of zinc coating holds significant importance, as numerous products in the aerospace industry rely on this method of joining.[13] Another crucial attribute is the lower density of zinc compared to steel. Achieving equivalent mechanical properties to high-strength steel while utilizing zinc can lead to reduced fuel consumption and environmental emissions. Zinc-based coatings are frequently used to reduce the risk of corrosion by two mechanisms: barrier protection and galvanic protection. However, when exposed to industrial pollutants and acidic or alkaline environments, they become vulnerable to wear and corrosion.

The aerospace industry employs a diverse array of advanced fabrication techniques to deposit coatings effectively depending on the desired physical and chemical properties to be attained. These techniques ranging from thermal spraying to physical vapor deposition, help achieve the demanding challenges of modern aviation.[14,15] Before choosing the deposition technique there are some factors to consider in order to achieve the desired finish. Surface preparation and cleaning are crucial to guarantee adhesion, and selecting the right coating material will ensure good adhesion and chemical affinity.[16,17] The temperature and pressure required for the process need to be compatible with the base material.[18] Elevated temperatures facilitate diffusion but can also affect the microstructure, impacting factors such as grain size, orientation, and crystallinity. Among all, electrochemical methods are the most economical option, demonstrating cost-effectiveness, good control of thickness and morphology ($\approx$25–100 nm), and a rapid deposition rate ($\approx$240 μm thickness in 1 h).[19] Complex morphologies can be achieved through electrochemical deposition because the result is always an even coating all over the surface. The use of room temperature avoids the irreversible phase transformation, thermal softening or shape-changing that occurs to most metallic substrates during deposition.

Klekotka *et al.*[20] electrodeposited Zn and Zn-metal oxide nanoparticle (Zn-NP) composite coatings and studied the hardness and tribological properties of the coatings using loads 1 and 2 N with frequencies of 5 and 10 Hz. Enhanced hardness (124 HV) and wear resistance (COF 0.68) for the coatings with hard particles were obtained when compared to that of a bare Zn coating (112 HV hardness and COF 0.79). The improved properties of nanoparticle-added Zn coatings were due to the easy protrusion of hard nanoparticles from the matrix and bearing of load during the tribological investigations.

Ramanauskas *et al.*[21] studied the microstructure and corrosion properties of electrodeposited zinc-based coatings, focusing on the structural modifications and corrosion behavior after heat treatments. The zinc alloys are Zn–Co, Zn–Fe, and Zn–Ni. The electrodeposition is performed in an alkaline cyanide-free plating solution over low-carbon steel samples. Subsequently, they are subjected to an annealing process at 225 °C under vacuum conditions. They used atomic force microscopy for surface morphology examination, X-ray diffraction to measure lattice parameters and phase composition, and direct current electrochemical methods to evaluate corrosion resistance. The process of annealing produces structural changes, intermetallic Fe/Zn compounds are formed, the lattice parameters are modified, and the amorphous oxide inclusions are transformed into crystalline. However, the corrosion behavior is not significantly modified in Zn, Zn–Co, and Zn–Fe coatings, while in Zn–Ni alloys there is a reduction in the diffraction peak width and the corrosion current is increased due to the formation of a more ordered lattice. This demonstrates that the corrosion resistance alters inconsistently for different alloy compositions.

The studies related to the fabrication, mechanical and tribological analyses of zinc composite coatings are very limited in the literature. Although diamond particles exhibit significant characteristics, the study of diamond-added coatings is a lacuna in the literature and needs more investigations. Therefore, herein, diamond nanoparticle-reinforced zinc composite coatings are prepared using electrochemical deposition. The concentration of diamond is varied from 0–10 g l^{-1}. The tribological properties of zinc-diamond composite coatings are reported for the first time in the present work. The optimum concentration of diamond is evaluated considering the hardness and wear resistance of the coatings. The mechanism of wear properties of the coatings is explored in the present study. Moreover, the present work interconnects the above-mentioned experiments with theoretical exploration, which is done by performing *in silico* studies to get a vibrant vision of the geometrical, structural and electronic features of Zn–diamond coatings. Thus, the current investigations bridge the gap between the theory and practice and show strong bonding and enhanced wear resistance of diamond-structured composite coatings for aerospace and automotive applications.

2. Materials and methods

2.1 Experimental studies

2.1.1 Electrodeposition of coatings. The electrodeposition of bare Zn and Zn-based composite coatings was carried out in an electrochemical cell using a direct current power supply (Fig. 1). To start the deposition process, stainless steel was prepared by using a 10% HCl solution followed by the polishing of the samples with different grit emery papers. Prior to immersion in the electrolytic solution, the samples were

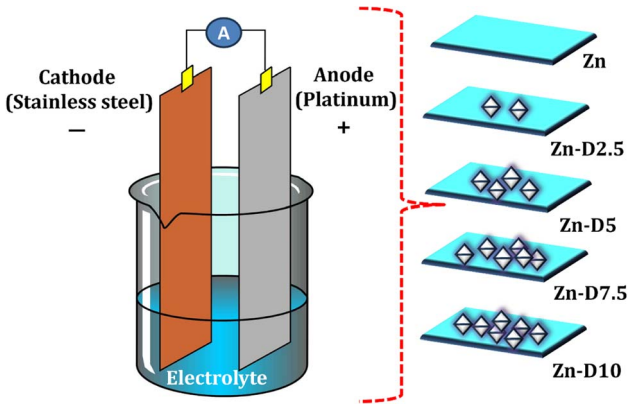

Fig. 1 Schematic representation of the fabrication process of Zn-diamond composite coatings.

washed with deionized water. The electrolyte was prepared by using 150 g l^{-1} $ZnSO_4 \cdot 7H_2O$, 30 g l^{-1} sodium sulphate (Na_2SO_4) 10 g l^{-1} NaCl and 0.05 g l^{-1} sodium dodecyl sulphate at an acidic pH 2–3, using a magnetic mixer at 200 rpm. Stainless steel was used as the working electrode or cathode while platinum was used as the anode or counter electrode (Fig. 1). The concentration of diamond was varied as 0 g l^{-1}, 2.5 g l^{-1}, 5.0 g l^{-1}, 7.5 g l^{-1} and 10 g l^{-1}. The diamond was added separately in the electrolyte to prepare the five types of coatings named bare Zn (Zn), Zn with 2.5 g l^{-1} diamond (Zn-D2.5), Zn with 5 g l^{-1} diamond (Zn-D5), Zn with 7.5 g l^{-1} of diamond (Zn-D7.5) and Zn with 10 g l^{-1} diamond (Zn-D10). The electrolytic bath for each coating will last 30 minutes at a cell voltage of 5.0 V and a current density of 100 mA cm^{-2} at constant room temperature. All chemicals were procured from Sigma Aldrich and the diamond powder was purchased from Dev Tech India, Maharashtra, India.

2.1.2 Physiochemical characterization of coatings. A scanning electron microscope (FE-SEM model Ultra 55 Carl Zeiss) was used to observe the topmost surface morphology of electrodeposited coatings. An X-ray diffractometer (XRD, Rigaku SmartLab) was used for the evaluation of the phases present in the composite coatings. The samples were scanned at a Cu-Kα wavelength of $\lambda = 1.5417$ Å in the 2θ range of 20–80°. A scan rate of 3° min^{-1} was applied with a step size of 0.02° during the testing.

2.1.3 Mechanical strength of the coatings. Hardness is the material's resistance to surface deformation, such as scratch or indentation. It is a measure of the material's ability to withstand localized plastic deformation or penetration by a pointed tool. The hardness provides insight into wear and abrasion resistance. There are many methods for measuring hardness, including Rockwell, Brinell, Vickers or pendulum hardness tests. In steel, hardness and tensile strength are roughly proportional. It is important to note that tensile strength and hardness are distinct mechanical properties that characterize different aspects of the material's behavior under different types of mechanical stress.[22] The Rockwell test measures the depth of penetration of an indenter under a large load compared to the penetration made by the preload. The preload sets the zero position, and subsequently, a gradual load is applied until the maximum pressure is reached. The maximum penetration pressure is recorded. The applied force is removed until the zero position is reached again. The hardness number is expressed by the symbol HRC and the scale designation. The hardness was measured with 60 kgf load on the coatings. Furthermore, the pendulum hardness test (König pendulum) was applied to all the Zn-diamond composite coatings to determine the consistent dispersion of diamond particles in the Zn matrix related to ASTM D4366 (as the hardness can be influenced by the dispersion of diamond particles). The number of oscillations that a pendulum resting on a coated surface would experience until its amplitude dropped by a predetermined amount was counted. The hardness decreases with the number of oscillations.

2.1.4 Tribological studies. Friction and wear performance of coating materials are very crucial to investigate the strength and endurance of the materials. A macro-tribometer was used for this purpose having a ball-on-flat type functionalization with a DC motor. The DC motor produced reciprocation motion during the experiments. The stroke length was 1.0 mm, and 9 Hz frequency and 1 N load were used during the testing.[23,24] For zinc coatings, a steel ball 6 mm in diameter acted as a counter body. The total reciprocations were 900 with 300 per minute. The wear experiment produced a lot of wear debris from the coating, which was removed using ethanol and the extent of demolition in coatings was detected by observing the morphology of the wear scars using SEM.

2.2 Computational methodology

For achieving a better understanding and new insights into the structural, stability/energetics, and electronic features of the diamond (two types) and their corresponding composite models, an *in silico* approach has been executed using a broadly used electronic structure calculation package Gaussian 09 installed at a Linux workstation.[25] The density functional theory (DFT) level of approach has been applied for the quantum chemical calculations where B3LYP is the functional for both the metal and non-metals and 6-31G (d,p) is the basis set for the non-metal C and H atoms and the LANL2DZ for the metal atom (Zn).

3. Results and discussion

3.1 Experimental analysis

3.1.1 Surface morphology and phase of composite coatings. The top surface morphology of Zn composite coatings is presented in Fig. 2. A bare Zn coating (Fig. 2a) shows a crystal of zinc with flower-like morphology. The addition of diamond particles in the zinc matrix resulted in the accumulation of diamond particles within the Zn matrix. Fig. 2b displays mostly Zn crystals while the dispersion of diamond is rarely visible in the coatings due to the lower concentration of diamond (2.5 g l^{-1}). The increased concentration of diamond (5 and 7.5 g l^{-1}) led to enhanced diamond content in the Zn matrix with proper

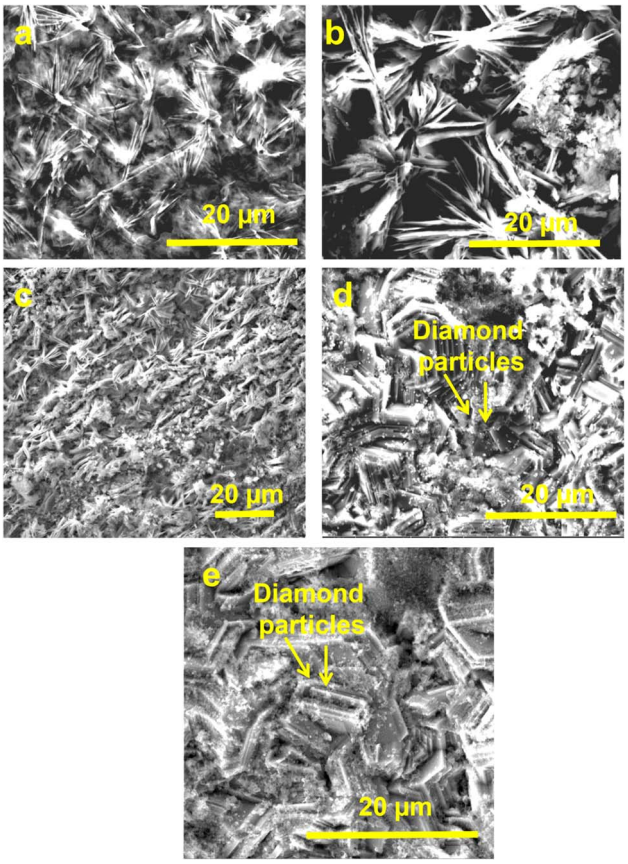

Fig. 2 Scanning electron microscopy images of (a) Zn, (b) Zn-D2.5, (c) Zn-D5, (d) Zn-D7.5 and (e) Zn-D10 composite coatings.

dispersion (Fig. 2c and d). Moreover, further increment in the concentration after 7.5 g l^{-1} (10 g l^{-1}) of diamond produced a larger number of diamond particles, which was attributed to the agglomeration of diamond in the Zn matrix (Fig. 2e). Similar SEM images of Zn coatings were reported by Khan *et al.*[26] and Almeida *et al.*[27] with the incorporation of silica and glycol within the Zn matrix. The digital camera images of the Zn composite coatings are given in the ESI (Fig. SI 1).†

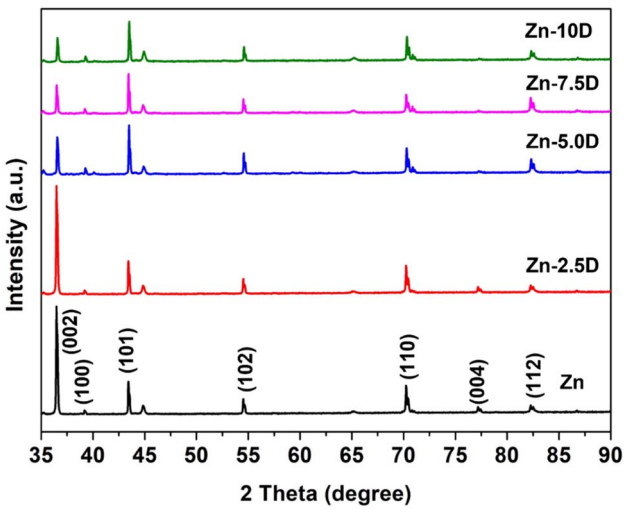

Fig. 3 XRD pattern of Zn and Zn-diamond composite coatings.

The XRD plot presented in Fig. 3 reveals the phases present in Zn composite coatings. The diffractogram exhibited characteristic peaks of Zn with crystallographic planes of (002), (100), (101), (102), (110), (004) and (112) at 2θ of ~36.14°, ~39.34°, ~43.29°, ~45.11°, ~54.91°, ~71.50°, ~77.01° and ~81.90° respectively. The XRD pattern was utilized further for the calculation of the crystallite size (t) of the composite coatings by using Scherrer's equation. The calculations were performed by using full width at half maxima (FWHM, β), Bragg's diffraction angle (θ), a constant k (0.9) and the X-ray's wavelength.

$$t = \frac{k\lambda}{\beta \cos \theta} \quad (1)$$

The crystallite size was obtained to be a minimum for Zn-D7.5 coating (21 ± 1 nm) due to the well-dispersed diamond particles. However, the crystallite size was enhanced for bare Zn (32 ± 2 nm) and Zn-D10 composite coatings (34 ± 2 nm) due to the larger crystal size as well as agglomerated diamond in the Zn-D10 coating (Table 1).

3.1.2 Mechanical and tribological studies. The mechanical strength of the coatings was determined using a Rockwell and pendulum hardness tester, which revealed that the 7.5 g l^{-1} diamond coating sustained the load more significantly with the highest hardness (70 HRC and 152 s from Rockwell and pendulum hardness, respectively) (Table 1). The hardness was minimal for bare Zn (58 HRC and 89 s from Rockwell and pendulum hardness, respectively) and Zn-D10 composite coatings (59 HRC and 102 s from Rockwell and pendulum hardness, respectively). The Zn-D2.5 (62 HRC and 119 s from Rockwell and pendulum hardness, respectively) and Zn-D5 (66 HRC and 149 s from Rockwell and pendulum hardness, respectively) composite coatings showed hardness less than that of Zn-D7.5 but higher than that of bare Zn and Zn-D10 coatings.

Further investigations on the load-bearing capacity of diamond-structured Zn coatings also disclosed Zn-D7.5 composite coating to be an ideal coating with an optimum concentration of 7.5 g l^{-1} of diamond in the Zn matrix. The results illustrate a reduced coefficient-of-friction (COF) for Zn-D7.5 (0.21) and Zn-D5 (0.28) coatings, which started increasing for bare Zn (0.44) as well as Zn-D10 (0.41) composite coatings (Table 1). However, the work on Zn–diamond coatings is completely missing in the literature but the studies based on the Zn coatings with other additives are reported here for the valuable assessment of the readers. The hardness and COF obtained in the current work are much improved than those in other reported work on Zn coatings. For instance, Tafreshi *et al.*[28] electrodeposited Zn–Ni coatings with varying concentrations of Ni in the Zn matrix. The hardness was reported to be maximum (293 HV) for 17 wt% Ni in the Zn matrix while in our case the highest achieved hardness is 70 HRC or 1150 HV.

Furthermore, Tafreshi and co-workers[28] reported a reduced COF (0.53) for the Zn with 14 wt% of Ni but the Ni-D7.5 composite coating prepared in the current work exhibited

Table 1 Crystallite size, hardness, COF and dissipation energy of the Zn-diamond composite coatings

Coatings	Crystallite size (nm)	Rockwell hardness (HRC)	Pendulum hardness (s)	COF	Dissipation energy ($\times 10^{-4}$ J)
Zn	32 ± 2	58	89	0.44 ± 0.06	8.8
Zn-D2.5	23 ± 1	62	119	0.33 ± 0.05	6.6
Zn-D5	24 ± 1	66	149	0.28 ± 0.03	5.6
Zn-D7.5	21 ± 1	70	152	0.21 ± 0.01	4.2
Zn-D10	34 ± 2	59	102	0.41 ± 0.04	8.2

a more reduced COF of 0.21. Also, Klekotka *et al.*[20] fabricated Zn and Zn coatings with hard nanoparticles and reported the highest hardness of 124 HV (in the present case 1150 HV) and a reduced COF up to 0.68 (0.21 in the present study). Thus, it can be perceived from the current research that the electro-deposited Zn-diamond coatings with specified parameters instigated improved friction resistance compared to that in other reported studies in the literature.

Dissipated energy is basically the energy released due to the damage of materials during the loading and unloading procedure, which influences the wear volume of the materials. The dissipation energy (U_f) is calculated by using the COF (μ), stroke amplitude (l) and applied load (F_N)

$$U_f = 2\mu F_N l \quad (2)$$

The results showed that the least energy was dissipated for the Ni-D7.5 coating during the wear test (4.2×10^{-4} J). The dissipation energy was calculated to be maximum for bare Zn (8.8×10^{-4} J) and Zn-D10 (8.2×10^{-4} J) coatings. The dissipation energy for Zn-D2.5 and Zn-D5 were calculated to be 6.6×10^{-4} J and 5.6×10^{-4} J, respectively (Table 1).

SEM was performed on the damaged coatings and their cross-sections to investigate the extent of wear produced during tribological experiments (Fig. 4). It can be seen from the images that bare Zn and Zn-D10 coatings have a larger scar (radius 0.29 mm and 0.25 mm, respectively) with a severe extent of delamination, formation of adhesive grooves and cracking of tribo-layers with high content of wear debris around the scars (Fig. 4a–j). The Zn-D2.5 composite coating showed some adhesive grooves over the scar (Fig. 4b–g) while a mild delamination can be detected in the Zn-D5 composite coating (Fig. 4c–h). The coating with 7.5 g l^{-1} of diamond concentration (Fig. 4d–i) exhibited smooth smearing in the scar by the counter body, devoid of any crack, groove or delamination of the tribo-layer. The scar of Ni-D7.5 is very narrow with a radius of ~0.16 mm. The failure of the material's surface during wear testing can be caused by four distinct regimes: (i) regime of mixed stick–slip, (ii) stick regime, (iii) regime with gross slip and (iv) reciprocating sliding regime.[24] The nucleation and propagation of cracks in the wear scar during wear testing are due to the stick slip, while the gross regime and stick regime are attributed to the removal of the surface from the coating. In the Zn–diamond coatings, cracks are present on the surface of coatings, so the wear of the Zn–diamond coatings is basically accompanied by the stick–slip regime.

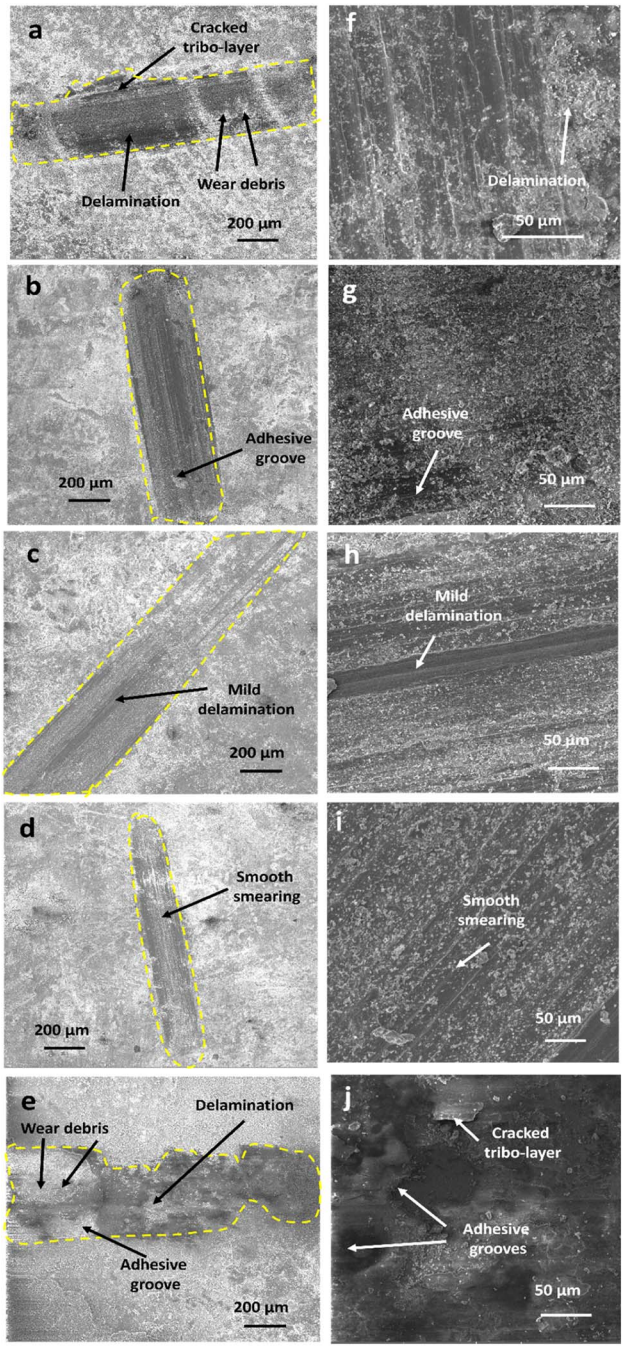

Fig. 4 SEM images of wear scars and cross-section of wear scars, respectively for (a and f) Zn, (b and g) Zn-D2.5, (c and h) Zn-D5, (d and i) Zn-D7.5 and (e and j) Zn-D10 composite coatings.

The wear volume of the composite coatings was calculated by using the measurements of wear scars such as the wear scar width (b), the depth of the wear scar (t) and wear track radius (r).[29]

$$W_v = \frac{2\pi tr}{6b}\left(3t^2 + 4b^2\right) \quad (3)$$

The wear volume for Zn is about 80% higher than that for the Zn-D7.5 composite coating and about 75% more than that for Zn-D2.5 (Table 2). The wear volume was the least for Zn-D7.5 (1.12×10^{-3} mm^3) while after increasing the concentration beyond 7.5 g l^{-1} of diamond, the wear volume started increasing (3.71×10^{-3} mm^3). The wear volume was further utilized for the calculations of the wear rate for the coatings.

$$W_r = \frac{\text{wear volume}}{\text{number of cycles} \times \text{stroke length} \times \text{load}} \quad (4)$$

The trend of the wear rate is the same as that of the wear volume for all the coatings. The wear resistance was observed to be the highest with a reduced wear rate for the Zn-D7.5 coating (1.25×10^{-3} mm^3 N^{-1} m^{-1}) while the least wear resistance or a high wear rate was found for Zn (8.45×10^{-3} mm^3 N^{-1} m^{-1}) and Zn-D10 composite coatings (4.13×10^{-3} mm^3 N^{-1} m^{-1}). The wear rate for Zn-D2.5 and Zn-D5 composite coatings was almost similar, which was less than that of Zn and Zn-D10 but higher than that of Zn-D7.5 coatings (Table 2). The wear resistance for Zn–diamond coatings is comparatively more improved than that of other Zn coatings, as reported in the literature. Tafreshi *et al.*[28] fabricated Zn and Zn–Ni composite coatings using electrodeposition and tested them for hardness, COF and wear volume. The least volume loss was reported for the Zn-14 wt%Ni (0.081 mm^3) coating. Praveen *et al.*[30] also reported the wear loss for Zn composite coatings to be 4 mg. Thus, reported values of hardness, COF, wear volume or wear rate are significantly higher than those presented in the current studies (Table 2). The bare Zn coating offered direct contact between the Zn coating and the steel counter body, which caused an enhanced wear rate and thus high wear in bare Zn (Fig. 5). The Zn-D10 coatings showed agglomerated diamond in the Zn matrix and introduced low wear resistance with cracks, ploughing and cutting of the coating surface (Fig. 5). The Zn-D2.5 and Zn-D5 composite coatings possessed a low content of diamonds, and cannot contribute to the strengthening of the matrix (Fig. 5). Conversely, Zn-D7.5 with optimum 7.5 g l^{-1} diamond showed a perfect dispersion of diamond in the Zn matrix which restricted the direct contact of the coating with the counter body as well as strengthened the matrix and provided enhanced load-bearing capacity of the coating. The well-dispersed diamond particles afforded strong mechanical interlocking and bonding with Zn; therefore, the exclusion of tough diamond particles from the Zn matrix by the counter body is very hard (Fig. 5). Fig. 5 shows the schematic representation of the wear mechanism for all Zn–diamond coatings.

3.2 Computational analysis

Several studies on the structural, stability and electronic feature analyses can be viewed in the literature which provide various useful information.[23,31] In chemical terminology, adamantane ($C_{10}H_{16}$), a well-known diamondoid is a variant of the carbon cage molecule, is also the smallest unit cage structure of the diamond crystal lattice. Diamondoids act as a model system for advanced electronic structure calculations because of their well-defined size and structure. Very interestingly, the E_{gap} obtained from the difference between the highest occupied molecular orbital (HOMO) and lowest unoccupied molecular orbital (LUMO) of the frontier molecular orbital (FMO) determines several optoelectronic features where the HOMO demonstrates the bulk state and the LUMO demonstrates the surface state. In this research work, both cases of diamond (with H, referred to as $C_{10}H_{16}$ and without H, denoted as C_{10}) have been chosen as parent component models. The optimized structures of both configurations are displayed in Fig. 6 (see the top left for the D with H and the top right for the D without H). Having a look into the experimental facets followed by diamond-structure zinc composite coatings, a foreign metal (Zn) is anchored with both diamond D (with and without H) moieties using the molecular modelling approach and then electronic structure calculations have been performed using the quantum mechanical approach.

In this research work, two composite models have been adopted to understand the geometrical/structural properties and stability/energetics portrayed by the binding interaction between two components (diamondoid consisting of C and H atoms, a constituent unit of diamond) or diamond (with C and without H) and the Zn metal. Here in this report, the former one zinc-diamond composite, Zn-D (with H) and the latter one zinc-diamond composite Zn-D (without H) with optimized structures are shown in Fig. 6 (bottom, left and right), respectively. In the case of Zn-D (with H: $C_{10}H_{16}$), the bond length of the Zn–C bond

Table 2 Characterization from tribological testing of electrophoretically deposited coatings

Coatings	Wear depth (t, mm)	Wear track radius (r, mm)	Wear scar width (b, mm)	Wear volume ($\times 10^{-3}$ mm^3)	Wear rate ($\times 10^{-3}$ mm^3 N^{-1} m^{-1})
Zn	0.0057	0.29	1.1	7.62 ± 0.1	8.45
Zn-D2.5	0.0032	0.21	1.1	3.02 ± 0.6	3.34
Zn-D5	0.0020	0.16	1.1	2.84 ± 0.1	3.16
Zn-D7.5	0.0014	0.14	1.1	1.12 ± 0.1	1.25
Zn-D10	0.0033	0.25	1.1	3.71 ± 0.7	4.13

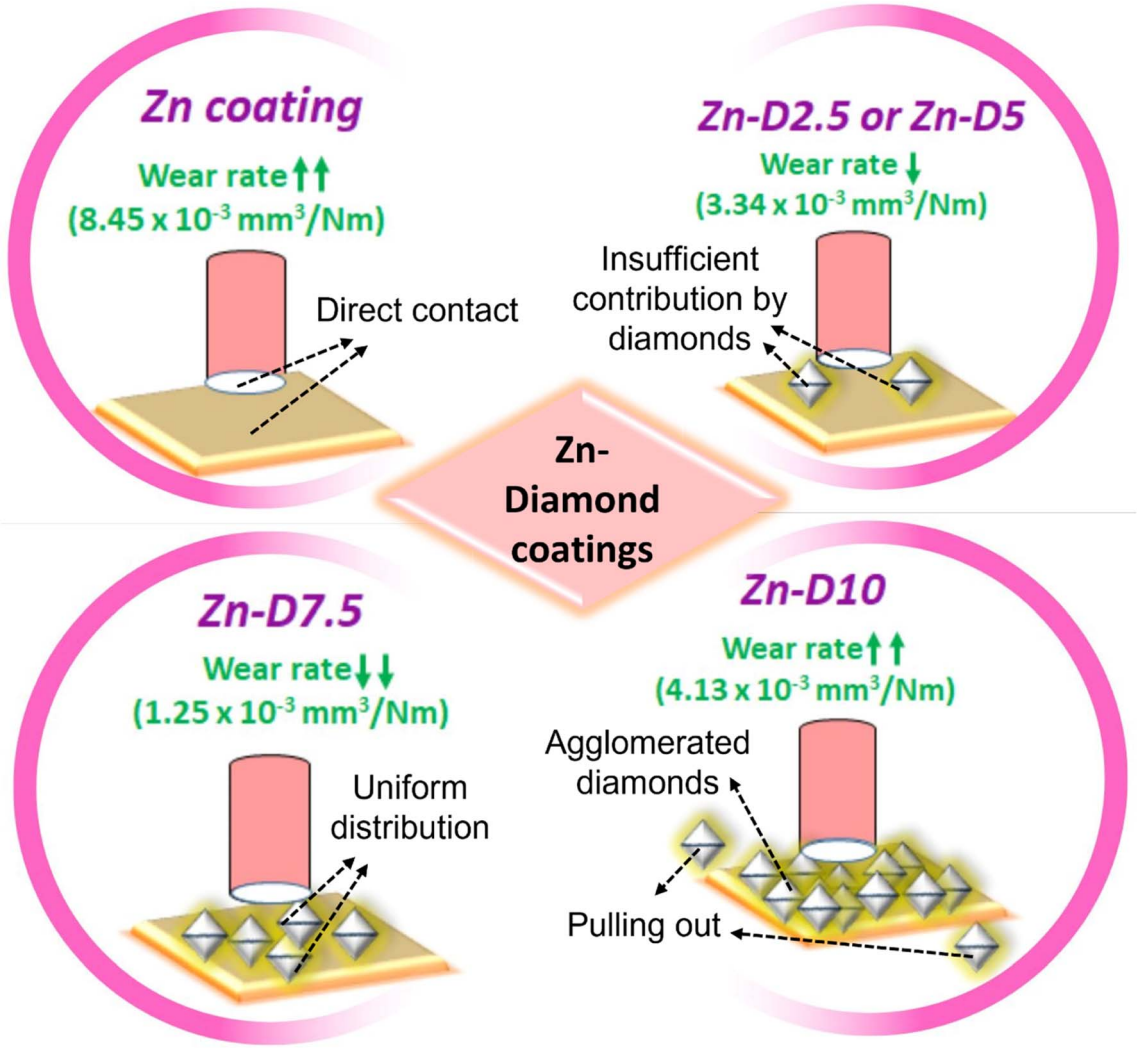

Fig. 5 Schematic representation of the wear mechanism of Zn, Zn-D2.5, Zn-D5, Zn-D7.5 and Zn-D10 composite coatings.

is calculated to be 2.3 Å whereas a reduced bond length for the same metal–nonmetal bond (without H: C_{10}) has been found to be 2.204 Å which could be due to significant interaction (d–p overlap) between the d-orbital of Zn metal and p-orbital of the carbon framework of diamond (without H) components. Importantly, for the Zn-doped diamond (C_{10}@Zn) (*i.e.* without H), the ∠Zn–C–C bond angles have been found to be 130.8° and 120.1° whereas the ∠Zn–C–C angle for the Zn-doped diamond ($C_{10}H_{16}$@Zn) (*i.e.* consisting of H atoms) has been observed to be 108.1° for all three bond angles and can be viewed in Fig. 6. Such observations show that the Zn-D (without H) composite model gives an indication of stronger metal–nonmetal interaction (MNI) (Zn–C bond) than that in the Zn-D (with H) composite model. In order to examine the binding interaction between the Zn metal and diamond, a supramolecular approach has been deployed for the calculation of binding energy (BE). It is surprising to note that the BE was found to be positive (showing an endothermic reaction and is thermodynamically not favourable) with a large 418 kcal mol^{-1} value in the case of the first configuration ($C_{10}H_{16}$@Zn), Zn-D consisting of H atoms (*i.e.* an adamantane constituting unit) while in the second configuration (C_{10}@Zn), it was detected to be negative, −33.3 kcal mol^{-1} (indicating an exothermic reaction and is thermodynamically stable). Importantly and very interestingly, the latter composite, Zn-D (without H) (having negative BE) is revealed to be more stable than the former one, Zn-D (without H); however, optoelectronic features also were in a similar order which is discussed below.

Moreover, as marked above about the role of the HOMOs and LUMOs of a material, such electronic parameters have been calculated along with acquiring their HOMO–LUMO energy gap (E_{gap}) as a diagnostic of the extent of photoelectron excitation. The exclusion of H atoms from the diamond, Zn-D (without H) indeed reduced the E_{gap} value (1.86 eV) which could be due to the engagement of delocalized pi-electrons therein; however, the E_{gap} is found to be larger (3.85 eV) in the case of Zn-D, (with H). The second configuration, Zn-D (without H) appears to show better optoelectronic properties because of having a low E_{gap}

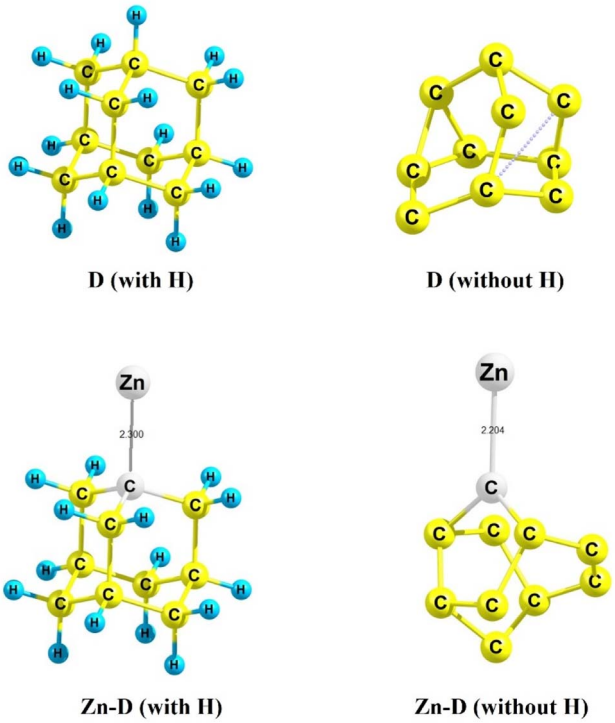

Fig. 6 Optimized structures of diamond-D (with and without H) and Zn-D (with and without H).

value, *i.e.* easy excitation of the photoelectrons from the HOMO to LUMO level. Such a finding is also favoured by the higher HOMO value (−5.529 eV) of the Zn-D (with H) as compared to that (−4.269 eV) of the Zn-D (without H).

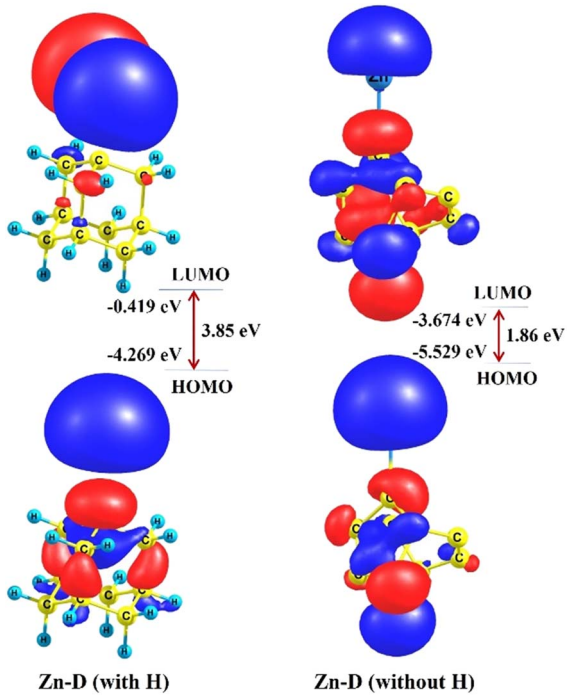

Fig. 7 HOMO and LUMO isosurface maps of the zinc-diamond (Zn-D) composite models (with and without H).

Furthermore, in order to have new insight into the contribution of FMOs (HOMOs and LUMOs) during the photoelectron excitation process, three-dimensional isosurface maps have been plotted. In the case of Zn-D (with H), the HOMOs are spread over a few C–C bonds of the diamond unit including the Zn metal; however, the LUMOs are located over only the Zn metal which appears to show a singly occupied molecular orbital (SOMO) as discerned from Fig. 7 (see bottom left for the HOMO and top left for the LUMO).[32]

For the same composite model, the charge on the Zn metal has been calculated to be positive (0.308*e*) whereas the charge on the diamond was negative (−0.308*e*) and this demonstrates that charge transfer (CT) can occur from metal (Zn) to the diamond unit. The HOMOs for the second composite model, Zn-D (without H) appeared to be localized over the CC bond which is almost similar to the Zn-D (with H) case, while the LUMOs are spread in a different pattern which can be seen from Fig. 7 (see bottom right for the HOMO and top right for the LUMO). Most importantly, natural atomic charge (+0.471*e*) on the Zn metal was detected to be enhanced in the case of the second configuration, Zn-D (with H); however, it was negative (−0.471*e*) on the diamond constituent unit which shows that the CT process also takes place from the Zn metal to the diamond unit, since the CT occurs from metal (Zn) to the non-metal region (diamond unit).

4. Conclusions

Diamond particles were reinforced in a Zn matrix to enhance the strength and tribological performance of the coatings. The diamond concentration was varied from 0 to 10 g l^{-1} in the Zn matrix. The mechanical strength was found to be the highest for the Zn-D7.5 composite coating when compared to bare Zn, Zn-D2.5, Zn-D5 and Zn-D10 coatings. Further investigation was carried out to estimate the wear resistance of coatings. The Zn-D7.5 coating exhibited an enhanced wear resistance with reduced COF (0.21) and dissipation energy (4.2×10^{-4} J). The wear scars obtained during the tribological test were used to determine the wear volume and wear rate of the coatings. The minimum wear volume (1.12×10^{-3} mm^3) and wear rate (1.25×10^{-3} mm^3 N^{-1} m^{-1}) were identified for the Zn-D7.5 coating when compared to that of bare Zn (7.62×10^{-3} mm^3 and 3.16×10^{-3} mm^3 N^{-1} m^{-1}), Zn-D2.5 (3.00×10^{-3} mm^3 and 3.34×10^{-3} mm^3 N^{-1} m^{-1}), Zn-D5 (2.84×10^{-3} mm^3 and 3.16×10^{-3} mm^3 N^{-1} m^{-1}) and Zn-D10 (3.71×10^{-3} mm^3 and 4.13×10^{-3} mm^3 N^{-1} m^{-1}) coatings. The high hardness and load-bearing capacity for the optimum Zn-D7.5 coating was due to the strengthening mechanism offered by the well-dispersed diamond particles. In the case of bare Zn, the direct contact between the counter body and coating resulted in reduced wear resistance. The low content of diamonds in Zn-D2.5 and Zn-D5 cannot provide a significant contribution to the strengthening of the matrix and therefore, they showed low wear resistance. Moreover, for the Zn-D10 coating, the diamond particles pulled out from the matrix due to the agglomeration of diamond particles, which led to diminished wear resistance. In contrast to other coatings, the strong mechanical interlocking between the diamond and Zn matrix in

the Zn-D7.5 coating restricted the removal of diamond particles from the Zn matrix during the wear test. The strong interlocking of diamonds was further confirmed by the geometrical, bonding and electronic feature calculations of the Zn-diamond composite that showed a binding energy of −33.3 kcal mol^{-1}. Thus, the Zn-D7.5 composite coating with high hardness and load-bearing ability can be an advanced futuristic coating material for aerospace and automotive applications.

Conflicts of interest

There is no conflict of interest.

Acknowledgements

The authors thank the Department of Chemistry and Department of Mechanical Engineering, Manipal University Jaipur. SA and SKP also acknowledge the Manipal Academy of Higher Education (MAHE) for providing a Manipal Research Board (MRB) seed grant. The authors thank Dr Ajay Saini for assisting during the coating preparation.

References

1 V. Balasubramanian, O. Niksan, M. C. Jain, K. Golovin and M. H. Zarifi, Non-destructive erosive wear monitoring of multi-layer coatings using AI-enabled differential split ring resonator based system, *Nat. Commun.*, 2023, **14**, 4916, DOI: **10.1038/s41467-023-40636-9**.

2 S. Invernizzi, F. Montagnoli and A. Carpinteri, Fatigue assessment of the collapsed XXth Century cable-stayed Polcevera Bridge in Genoa, *Procedia Struct. Integr.*, 2019, **18**, 237–244, DOI: **10.1016/j.prostr.2019.08.159**.

3 E. O. Obanijesu, V. Pareek, R. Gubner and M. O. Tade, Corrosion education as a tool for the survival of natural gas industry, *Nafta*, 2010, **61**, 553–563.

4 C. M. Hansson, *Corrosion of Steel in Concrete Structures*, ed. A. Poursaee, Elsevier, 2016.

5 H. Mughrabi, Fatigue, an everlasting materials problem - still en vogue, *Procedia Eng.*, 2010, **2**, 3–26, DOI: **10.1016/j.proeng.2010.03.003**.

6 U. H. Tiong and G. Clark, The structural environment as a factor affecting coating failure in aircraft joints, *Procedia Eng.*, 2010, **2**, 1393–1401, DOI: **10.1016/j.proeng.2010.03.151**.

7 H. Qiu, K. Feng, A. Gapeeva, K. Meurisch, S. Kaps, X. Li, L. Yu, Y. K. Mishra, R. Adelung and M. Baum, Functional polymer materials for modern marine biofouling control, *Prog. Polym. Sci.*, 2022, **127**, 101516.

8 S. Awasthi, C. P. Pandey and K. Balani, Synergistic role of carbonaceous reinforcements on multi length scale tribology of electrophoretically deposited nickel-boron nitride coatings, *Mater. Res. Bull.*, 2018, **99**, 61–72.

9 M. F. Mosser, *Metallic-Ceramic Coatings as Replacements for Cadmium Plating*, 1990, DOI: **10.4271/900968**.

10 A. Agüero, J. C. del Hoyo, J. García de Blas, M. García, M. Gutiérrez, L. Madueño and S. Ulargui, Aluminum slurry coatings to replace cadmium for aeronautic applications, *Surf. Coat. Technol.*, 2012, **213**, 229–238, DOI: **10.1016/j.surfcoat.2012.10.052**.

11 T. Zhang, T. Zhang, Y. He, Y. Wang and Y. Bi, Corrosion and aging of organic aviation coatings: A review, *Chin. J. Aeronaut.*, 2023, **36**, 1–35, DOI: **10.1016/j.cja.2022.12.003**.

12 S. Awasthi, S. Goel, C. P. Pandey and K. Balani, Multi-Length Scale Tribology of Electrophoretically Deposited Nickel-Diamond Coatings, *JOM*, 2017, **69**, 227–235, DOI: **10.1007/s11837-016-2142-4**.

13 A. R. Marder, The metallurgy of zinc-coated steel, *Prog. Mater. Sci.*, 2000, **45**, 191–271, DOI: **10.1016/S0079-6425(98)00006-1**.

14 J. G. H. Hermens, T. Freese, K. J. van den Berg, R. van Gemert and B. L. Feringa, A coating from nature, *Sci. Adv.*, 2020, **6**, eabe002–eabe0012, DOI: **10.1126/sciadv.abe0026**.

15 B. Fotovvati, N. Namdari and A. Dehghanghadikolaei, On Coating Techniques for Surface Protection: A Review, *J. Manuf. Mater. Process.*, 2019, **3**, 28, DOI: **10.3390/jmmp3010028**.

16 H. M. S. Iqbal, S. Bhowmik and R. Benedictus, Performance evaluation of polybenzimidazole coating for aerospace application, *Prog. Org. Coat.*, 2017, **105**, 190–199, DOI: **10.1016/j.porgcoat.2017.01.005**.

17 M. N. Khan, S. Shah and T. Shamim, Investigation of operating parameters on high-velocity oxyfuel thermal spray coating quality for aerospace applications, *Int. J. Adv. Des. Manuf. Technol.*, 2019, **103**, 2677–2690, DOI: **10.1007/s00170-019-03696-0**.

18 C. Donnet and A. Erdemir, Solid Lubricant Coatings: Recent Developments and Future Trends, *Tribol. Lett.*, 2004, **17**, 389–397, DOI: **10.1023/B:TRIL.0000044487.32514.1d**.

19 S. Awasthi, S. K. Pandey, C. P. Pandey and K. Balani, Progress in Electrochemical and Electrophoretic Deposition of Nickel with Carbonaceous Allotropes: A Review, *Adv. Mater. Interfaces*, 2020, **7**, 1901096–1901129, DOI: **10.1002/admi.201901096**.

20 M. Klekotka, K. Zielińska, A. Stankiewicz and M. Kuciej, Tribological and Anticorrosion Performance of Electroplated Zinc Based Nanocomposite Coatings, *Coatings*, 2020, **10**, 594, DOI: **10.3390/coatings10060594**.

21 R. Ramanauskas, R. Juškėnas, A. Kaliničenko and L. F. Garfias-Mesias, Microstructure and corrosion resistance of electrodeposited zinc alloy coatings, *J. Solid State Electrochem.*, 2004, **8**, 416–421, DOI: **10.1007/s10008-003-0444-2**.

22 J. T. Black and R. A. Kohser, *De Garmo's Materials and Processes in Manufacturing*, John Wiley & Sons, Inc, 13th edn, 2019.

23 S. Awasthi and K. Pandey, Load-bearing study and interfacial interactions of hydroxyapatite composite coatings for bone tissue engineering, *Mater. Chem. Front.*, 2022, **6**, 3731–3747.

24 S. Awasthi, J. K. Gaur and M. S. Bobji, Advanced Ferrogels with High Magnetic Response and Wear Resistance Using Carbon Nanotubes, *J. Alloys Compd.*, 2020, **848**, 156259–156269.

25 D. J. F. M. J. Frisch, G. W. Trucks, H. B. Schlegel, G. E. Scuseria, M. A. Robb, J. R. Cheeseman, G. Scalmani,

V. Barone, B. Mennucci, G. A. Petersson, H. Nakatsuji, M. Caricato, X. Li, H. P. Hratchian, A. F. Izmaylov, J. Bloino, G. Zheng, J. L. Sonnenberg and M. Had, *Gaussian 09*, Gaussian, Inc., Wallingford CT, 2009.

26 T. R. Khan, A. Erbe, M. Auinger, F. Marlow and M. Rohwerder, Electrodeposition of zinc–silica composite coatings: challenges in incorporating functionalized silica particles into a zinc matrix, *Sci. Technol. Adv. Mater.*, 2011, **12**, 055005, DOI: **10.1088/1468-6996/12/5/055005**.

27 M. D. de J. Almeida, C. A. Della Rovere, L. R. P. de A. Lima, D. V. Ribeiro and C. A. C. de Souza, Glycerol Effect on the Corrosion Resistance and Electrodeposition Conditions in a Zinc Electroplating Process, *Mater. Res.*, 2019, **22**, e20180480–e20180492, DOI: **10.1590/1980-5373-mr-2018-0480**.

28 M. Tafreshi, S. R. Allahkaram and H. Farhangi, Comparative study on structure, corrosion properties and tribological behavior of pure Zn and different Zn-Ni alloy coatings, *Mater. Chem. Phys.*, 2016, **183**, 263–272, DOI: **10.1016/j.matchemphys.2016.08.026**.

29 S. Wang, L. Zhou, C. Li, Z. Li and H. Li, Morphology and wear resistance of composite coatings formed on a TA2 substrate using hot-dip aluminising and micro-arc oxidation technologies, *Materials*, 2019, **12**, 799–816.

30 B. M. Praveen and T. V. Venkatesha, Electrodeposition and properties of Zn-nanosized TiO2 composite coatings, *Appl. Surf. Sci.*, 2008, **254**, 2418–2424, DOI: **10.1016/j.apsusc.2007.09.047**.

31 S. Awasthi, J. K. Gaur, S. K. Pandey, M. S. Bobji and C. Srivastava, High-Strength, Strongly Bonded Nanocomposite Hydrogels for Cartilage Repair, *ACS Appl. Mater. Interfaces*, 2021, **13**, 24505–24523, DOI: **10.1021/acsami.1c05394**.

32 S. K. Pandey, Novel and Polynuclear K- And Na-Based Superalkali Hydroxides as Superbases Better Than Li-Related Species and Their Enhanced Properties: An Ab Initio Exploration, *ACS Omega*, 2021, **6**, 31077–31092.